Observations of soot during droplet combustion at low gravity: heptane and heptane/monochloroalkane mixtures

G. S. JACKSON, C. T. AVEDISIAN and J. C. YANG†

Sibley School of Mechanical and Aerospace Engineering, Cornell University, Ithaca, NY 14853, U.S.A.

Abstract—Experimental observations of the combustion of sooting fuel droplets, performed in a drop tower to create a low gravity environment, are reported. Free n-heptane droplets and suspended droplets of heptane, monochloroalkanes, and mixtures of monochloro-octane and heptane were studied. Initial droplet diameters ranged from 0.4 to 1.1 mm. The results suggest that soot may influence droplet vaporization rates. Spherical symmetry of the flame allowed for extended observation of soot agglomerates inside the droplet flame. Effects of slight convective flows were also observed, both through variations of natural convection around the suspended droplets and through variations in the drift velocities of the unsupported droplets. Slight convective flows around the suspended droplets reduced flame luminosity as well as soot accumulation inside the flame and increased droplet vaporization rates. Mixing monochloro-octane with n-heptane demonstrated the effectiveness of n-heptane in reducing soot emissions from the flames of the chlorinated fuels. Finally, trends of initial droplet diameter with burning rate were observed and may be linked to the effect of droplet size upon soot formation inside the flame.

1. INTRODUCTION

ALTHOUGH analytical models provide significant insight into the physical processes of droplet combustion, their ability to accurately predict experimentally observable quantities such as burning rates and flame diameters is currently limited to fuels which have non-sooting flames. The presence of soot in the gas surrounding the droplet may alter the heat and mass transfer between the droplet and its flame, which in turn controls the burning rate and propensity for flame extinction. Current theories of droplet combustion do not account for the influence of soot. Recent experimental results of free/unsupported droplets burning in near spherically symmetric environments have underscored the potential importance of soot in droplet combustion [1–3]. Differences in the means of ignition, in convective flows around the droplets due to the various droplet deployment methods, or even in initial droplet diameters may have been responsible for reported differences in the experimental results by their effect on soot dynamics. In particular, the influence of initial droplet diameter may be noteworthy and is not addressed in the classical quasi-steady theory of droplet combustion [4]. The recent experimental results point to initial droplet diameter as affecting the extent of soot accumulation inside the droplet flame as well as the burning rate.

The present study was undertaken to further document the potential influence of soot on droplet burning characteristics. Qualitative influences of initial droplet diameter, fuel composition, and slight convective gas flows around the droplet on soot formation and accumulation were examined. The present experiments were performed in a near buoyancy-free (low gravity) environment with the droplets being nearly stationary in order to promote spherically symmetric burning. The near spherically symmetric environment also allows for greater sensitivity of parametric influences on soot formation because natural or forced convection does not rapidly sweep the soot through the flame. This experimental study was carried out in the hope of providing information for future improvements of droplet combustion models.

n-Heptane was selected as a test fuel for comparison with the extensive previous heptane droplet combustion studies at low gravity. Heptane droplets were also studied to assess the influence of recent experimental modifications on the burning process. Monochlorinated alkanes were studied because of their importance in the incineration of hazardous waste liquids. Finally, mixture droplets of n-heptane and monochloro-octane were burned in order to assess the influence of fuel composition upon sooting where both fuel mixture components are prone to form soot—although heptane significantly less so than monochloro-octane.

The experimental method employed both free-floating (i.e. unsupported) and fiber-supported droplets. The two means of droplet deployment yielded a two-fold range of initial droplet diameters—around 0.5 m for the unsupported droplets and 1 mm for fiber-supported droplets. This range resulted in observable

---

† Present address: Center for Building and Fire Technology, National Institute of Standards and Technology, Gaithersburg, MD 20899, U.S.A.

NOMENCLATURE

C_m momentum exchange coefficient ($= 1.14$ in model)

C_P specific heat capacity in the gas phase

C_s thermal slip coefficient ($= 1.17$ in model)

C_t kinetic theory coefficient for temperature jump at interface ($= 2.18$ in model)

D mass diffusion coefficient of fuel in the gas phase

d droplet diameter

F'_D dimensional Millikan drag force in the radial direction on stationary particle

F_D non-dimensional drag force in the radial direction on stationary particle

F_{TH} non-dimensional thermophoretic force in the radial direction

g acceleration due to gravity level

Gr Grashof number

K vaporization rate of droplet

R universal gas constant

Re Reynolds number

r radius

T temperature

t_F average residence time for fuel molecules in the gas phase

U non-dimensional momentum of particle in the radial direction

V radial diffusion velocity in gas phase

v velocity

W_i molecular weight of species i

Y_i mass fraction of species i.

Greek symbols

β thermal expansion coefficient

ζ net force on particle in the radial direction

λ mean free path

μ dynamic viscosity

ξ dimensionless position inside the droplet flame

ρ density

τ non-dimensional time.

Subscripts

d   droplet surface

F   fuel

f   flame position

g   gas phase

l   liquid phase

p   soot particle

∞ far ambient.

differences in burning rates and extents of sooting of *n*-heptane droplets which were attributed to initial diameter effects. The larger droplets experienced slight axial vapor flows in the latter period of combustion due to natural convection induced by an increase in air drag on the experimental package during free fall. This provided an opportunity to study the evolution of the droplet flame and soot structure caused by small axial vapor flows around the droplet.

2. EXPERIMENTAL DESCRIPTION

2.1. *Experimental technique and conditions*

Burning of both free unsupported droplets and droplets suspended from a small quartz fiber was observed. Free droplets were preferred because a suspension fiber may have disrupted soot structures above the droplet and influenced the potential for flame extinction or for microexplosion which can arise from internal boiling due to nucleation at the fiber surface. However, safety considerations encouraged the use of suspended droplets for the monochloroalkanes, because the suspended droplet method required less exposed fuel for the experimental set-up. Furthermore, the difficulty of obtaining perfectly stationary free droplets led to burning suspended droplets in the present study, but no data were taken near the end of burning when the droplets became too small.

Experiments were conducted in a drop tower facility, which has been described in detail elsewhere [3, 5, 6], to create a low-gravity ambience for droplet combustion. The drop tower provided 1.2 s of free fall. The experimental observation time was long enough to record the complete burning of the small free droplets studied and about 75% of the projected burning history of the larger supported droplets. The experimental drop package included the combustion chamber, ignition transformers, a high-speed movie camera, and a CCD video camera. Ambient conditions in the combustion chamber were 0.101 MPa and $25 \pm 2°C$.

Free unsupported droplets of *n*-heptane were produced by a droplet generator based upon the ink jet method. A droplet was captured in a relatively stationary configuration by shooting it vertically upward and releasing the experimental package into free fall as the droplet reached its apex. Droplets generated by this method had initial diameters ranging from 0.4 to 0.5 mm. Modifications of the free droplet experiment [6, 7] from previously reported experiments [3, 5] included ignition during free fall, subsequent removal of the electrodes from the vicinity of the burning droplet, and better control of the ambient gas composition around the droplet with a more open droplet generator design and thorough flushing of the combustion chamber before the experiment.

For monochloroalkane fuels and chloroalkane/

n-heptane mixtures, droplets were suspended on a bead at the end of a quartz fiber and then ignited on the fiber in the low-gravity environment. The fiber and bead diameters were 50 μm and 100 μm, respectively. Heat transfer through the fiber, which is approximately proportional to the fiber cross-sectional area, is expected to be negligible for such small fiber diameters. A simple analysis revealed that heat transfer through the fiber to a suspended heptane droplet would be less than 1% of the total heat transfer to the droplet calculated from the vaporization rate [8]. Suspended droplet diameters in this study ranged from 0.7 to 1.1 mm.

The spark ignition may have exerted a small influence on combustion. For the highly sooting monochloroalkanes flames, unnecessarily long spark discharges resulted in more soot agglomerates forming early in the combustion process (though without apparently affecting the entire combustion period). For this reason, the spark duration was kept near to the minimum for igniting the various fuels, ranging from 15 to 30 ms for the ignition system used in the present study. A noticeable reduction in soot accumulation, flame luminosity, and burning rate resulted if the electrodes were held near the flame during the entire combustion process. Nearby surfaces have been shown to suppress soot formation and flame luminosity and to reduce burning rates in droplet combustion [8]. Hence, the electrodes were retracted away from the flame. Electrode retraction sometimes induced a gas motion which drew the soot into a tail that protruded through the flame in the direction of retraction.

Due to air drag on the drop package, the gravity level experienced in the moving frame of reference did not remain constant but rather increased with time. The corresponding Grashof number (Gr) for the burning droplet, defined as

$$Gr(t) = \frac{\beta \Delta T \rho^2 g(t) d(t)^3}{\mu^2}, \qquad (1)$$

thus changed, not only from variations of the characteristic length scale in the experiment (i.e. the droplet diameter) but also from variations of gravity created by the build-up of air drag around the falling package.

Gr depends on physical properties and the time-dependent gravity level and droplet diameter. Gravitational acceleration was measured by an accelerometer which recorded gravity levels ranging from less than 10^{-4} of the earth's normal gravity to near 10^{-2} just before the end of free fall. Property values were evaluated for air at an arithmetic mean of the flame and ambient temperature. Instantaneous droplet diameters were calculated from the classical 'd^2 law' [4]

$$d^2 = d_0^2 - Kt \qquad (2)$$

where average burning rates for the liquids studied in

the experiments were used for K. Figure 1 shows the evolution of Grashof numbers for heptane droplets with two different initial diameters. Gravity levels were taken from a theoretical curve fit of the experimentally measured values. The maximum in Gr arises from the competing effects of a diminishing droplet diameter during combustion and an increasing gravity level during free fall with the present experiments. Figure 1 shows that a 0.5 mm diameter heptane droplet burns in the first 0.4 s of free fall and never experiences a Gr above 10^{-4}. On the other hand, a heptane droplet with an initial diameter of 1.0 mm does not burn to completion during the 1.2 s of free fall and has a Gr which increases to nearly 10^{-2} before decreasing.

2.2. Data reduction

High-speed movie records of burning droplets provided the primary data source. Two methods were used to extract data from the film records. The first method involved projecting the film image onto a horizontal plane and manually abstracting horizontal and vertical diameters. This method was used to obtain droplet diameter measurements for the suspended droplets. A detailed discussion of the errors involved in this technique for diameter measurements is given elsewhere [6].

The second method, used for the unsupported *n*-heptane data as given in Fig. 2, employed a computer-based image analysis package (Automatix Inc., Billerica, MA) for a frame by frame analysis. Each film image was magnified through a microscope onto a CCD camera which then sent the image to the computer for processing. Average diameters for the droplets were determined by setting a specific threshold gray level depending on the film background.

The two data reduction methods were compared for all the unsupported *n*-heptane droplet diameter data and the overall burning rate for heptane varied by less than 2%, which suggests that the manual method provided relatively accurate measurements. Both methods still have an element of subjectivity: defining the tangent to the boundary in the manual method and setting the gray level in the computer-based analysis. None the less, the computerized analysis is generally preferred because it allows for more repeatable measurements. However, due to the current inability of the software to define an appropriate boundary for the suspended droplets near the suspension fiber, the manual method was chosen for the data reduction of these droplets. The technique for defining the droplet boundary near the suspension fiber is discussed in an earlier reference [8].

3. EXPERIMENTAL RESULTS

3.1. *n*-Heptane

3.1.1. *Free droplets.* Free *n*-heptane droplets burned in the present study had initial diameters ranging from 0.43 to 0.49 mm. For these small droplets measured burning rates ranged from 0.71 to 0.82 mm^2 s^{-1} with
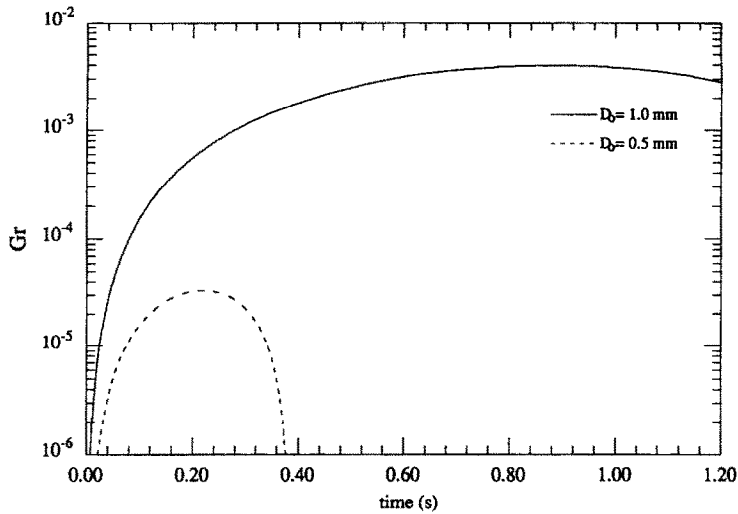
FIG. 1. Evolution of Grashof number vs time from free fall for n-heptane droplets with initial diameters of 0.5 mm and 1.0 mm.

an average of 0.75 mm^2 s^{-1} and a standard deviation of ± 0.04. The time periods used to calculate burning rates were chosen to exclude any initial period of droplet heating in the combustion process. Only data obtained with the present experimental set-up were used to calculate the average burning rate. Figure 2 shows dimensionless d^2 data from the computerized image analysis for the droplets used to calculate the burning rates. Some runs were excluded because of higher drift velocities, soot obscuring the droplet boundary for a significant period of the burning, or degradation in the focus of the droplet. The limited burning histories for some of the droplets in Fig. 2 are the result of those droplets drifting slightly out of focus or out of the camera field of view during burning.

The maximum Reynolds numbers for the unsupported droplets, based on droplet diameter and air properties at the mean temperatures of the flame and the far ambient, ranged from 0.03 to 0.12. These maximum Reynolds numbers were obtained from maximum droplet drift velocities which were approximately 10% or less of calculated radial Stefan flow velocities in the gas phase inside the flame. Instantaneous Reynolds numbers were generally an order of magnitude below these maximum values. For droplets such as those shown in the photographic sequence of Fig. 3, the Reynolds numbers were practically zero as the droplets became stationary after slight initial drifting. Although it has been suggested that the maximum velocity of the droplet relative to soot agglomerates formed during combustion should be
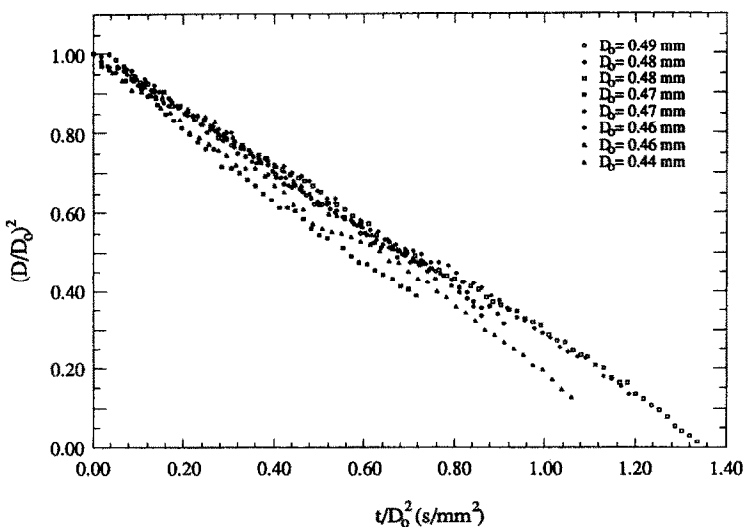

FIG. 2. Non-dimensional d^2 profiles vs time from ignition for unsupported n-heptane droplets burning at low gravity with minimal drift velocities.
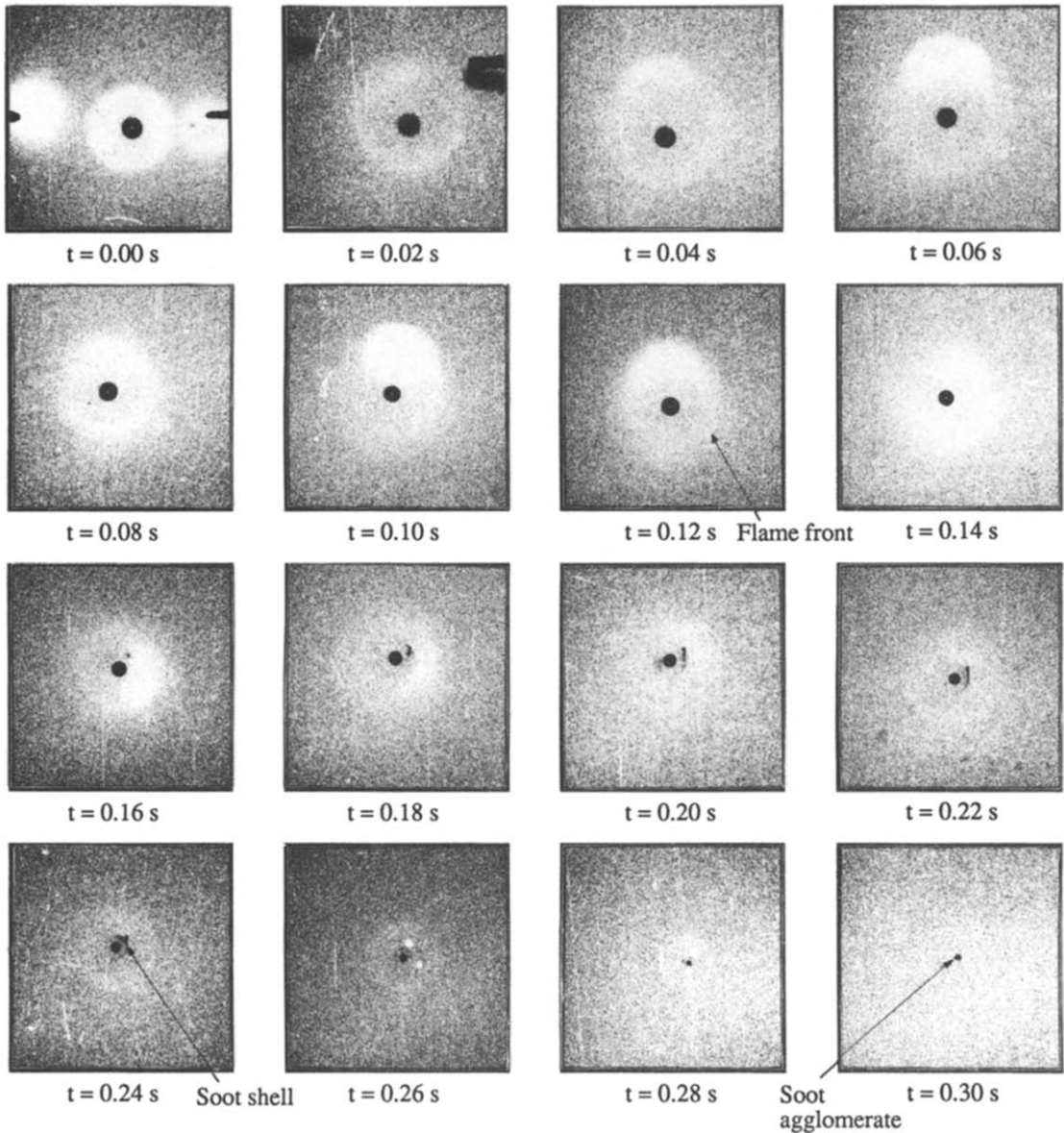
FIG. 3. Photographic sequence of unsupported n-heptane droplet ($D_0 = 0.47$ mm) burning at low gravity showing development of soot shell from $t = 0.18$ s to $t = 0.26$ s and soot agglomerate emission at end of burning, $t = 0.30$ s.

used for defining a Reynolds numbers to correlate burning characteristics [2], the small heptane droplets in the present study produced so little soot that it was difficult to track individual soot agglomerates. Thus, the Reynolds numbers were based upon the motion of the droplet relative to the ambient gas. From these results, no correlation was found between vaporization rates and the small Reynolds numbers in the present study.

All the heptane droplet flames observed in this study exhibited soot radiation. Unlike prior work [3, 5] where the intensity of backlighting drowned out the luminosity from soot radiation, the different lighting scheme of the present study revealed the soot radiation around the flame zone. For those droplets with very little drift, the flames remained spherical through-

out burning as the instantaneous Grashof number never rose above 10^{-4} (cf. Fig. 1). These flames were accompanied by the eventual formation of a nearly spherical shell of soot aggregates inside the flame. Figure 3 shows such a soot shell, visible from $t = 0.18$ s to $t = 0.26$ s. The soot shell was composed of soot particle agglomerates generated near the flame region and transported in toward the droplet to a region of mechanical equilibrium (cf. Section 4.2). The density of soot particles in this shell structure increased as combustion proceeded until near the end of burning when the flame began to shrink. The rapid shrinking of the flame would generally overtake the soot shell, resulting in some soot being oxidized. The flame was extinguished after the droplet appeared to completely vaporize and before all the soot was destroyed. This

resulted in a small amount of soot remaining un-oxidized as seen in the $t = 30$ s photograph in Fig. 3.

Droplets which maintained larger drift velocities did not necessarily develop a soot shell because soot formed inside the flame was convected behind the droplet and through the flame. Particles swept into the wake of the droplet were oxidized to some extent, though not necessarily completely. Soot swept in the wake of drifting droplets generally remained near the flame boundary and left an inner region where little soot was visible. As the droplet reduced in size and the flame became more spherical, soot particles were either emitted through the flame or formed a tail of agglomerates which extended through the flame.

3.1.2. *Suspended droplets.* Experiments performed on larger suspended heptane droplets with initial diameters ranging from 0.9 to 1.0 mm revealed an increase in soot production and accumulation during combustion with the larger droplet sizes. Figure 8(a) illustrates a typical example of a burning suspended heptane droplet. Soot shells were observed to initially form about 200 ms after ignition as with the smaller unsupported droplets.

The longer burning time for the larger droplets provided an opportunity for observing the influence of progressively increasing buoyant flows around the droplet due to the rise in gravity levels on the flame and soot structure in the latter half of the free fall. Between 0.45 and 0.55 s after ignition, buoyant flows disrupted the soot shell surrounding the suspended droplets and the flame became progressively non-spherical. The suspended heptane droplets experienced instantaneous Grashof numbers above 10^{-3} after 0.3 s into the burning period (cf. Fig. 1). This value appears to indicate an approximate threshold above which the influence of buoyancy becomes significant enough to distort the flame shape. The continued increase in Gr resulted in further distortion of the flame and soot structure. Figure 8(a) further shows that the soot shell became very faint as its shape became more distorted by natural convection, and eventually the accumulated soot was completely swept away with no visible agglomerates being formed after convection removed the shell. Even after distortion due to natural convection, the flames of the suspended heptane droplets appeared to maintain their envelope structure as indicated by the suspension fiber remaining illuminated in a thin region above the droplet near the apparent flame boundary.

Because of the progressive distortion of the soot structure and the flame caused by the increase in Gr during burning, only data from the time period when the flame and the soot shell maintained near spherical shapes were used for calculating the burning rates of the stationary suspended droplets. The average burning rate was observed to be 0.60 (± 0.01) mm^2 s^{-1}. This value is very close to the average burning rate (0.58 mm^2 s^{-1}) reported for similar-sized free-floating n-heptane droplets [2] and is 9% lower than the average burning rate reported for similar-sized suspended

heptane droplets at low gravity in another study [8], in which, however, data were also included from the time regime when the flame became significantly distorted. These differences may not be considered significant in light of the potential influences of soot on burning differences in the various experimental methods used to obtain the data.

3.2. *Monochloroalkanes*

Suspended monochloroalkane droplets produced significantly more soot than n-heptane droplets. This increase in soot production enhanced the observation of soot dynamics in the diffusion flame environment. The photographs in Fig. 4 show that the droplet flames of 1-chloropentane, -heptane, and -octane formed larger agglomerates, denser soot shells, and more luminous flames than the less sooting n-heptane flames.

In the early period of combustion of the mono-chloroalkane droplets, many soot agglomerates formed and were carried back toward the droplet surface where they further coagulated in a dense, reasonably spherical shell around the droplet. The soot shell became visible between 80 and 160 ms after ignition, a shorter delay time than with the less sooty n-heptane flames. The shell initially formed close to the droplet in a thin region with an average diameter less than twice the instantaneous droplet diameter. The shell maintained a relatively constant size with only a slight increase while the droplet continued shrinking due to vaporization. Of the chloroalkanes studied, the least volatile, monochloro-octane, seemed to form a soot shell closest to the droplet and chloro-pentane, the most volatile, formed a soot shell furthest from the droplet.

As in the case with the suspended heptane droplets, the Grashof number for the monochloroalkane droplets increased during combustion to the extent that natural convection began to drive soot particles upward through the flame after about 0.5 s from ignition. Significant amounts of soot collected in the shell structures before the increase in convective flows, but the buoyant flows eventually distorted and opened the flame from its envelope structure with soot agglomerates escaping through the 'hole' created in the flame—just as with droplets burning at normal gravity [9]. Some of this soot collected on the suspension fiber.

The burning rates of initially similar-sized mono-chloroalkane droplets under near spherically symmetric conditions decreased as the number of carbon atoms per molecule increased. Table 1 lists burning rates for the region after droplet heat-up and before convection distorted the flame for droplets with initial diameters ranging from 0.9 to 1.1 mm. Figure 5 shows dimensionless d^2 plots for droplets of the three monochloroalkane fuels, and the repeatability of the burning histories of similar-sized droplets of the same fuel is evident. In order to better illustrate the differences found for the various monochloroalkanes stud-
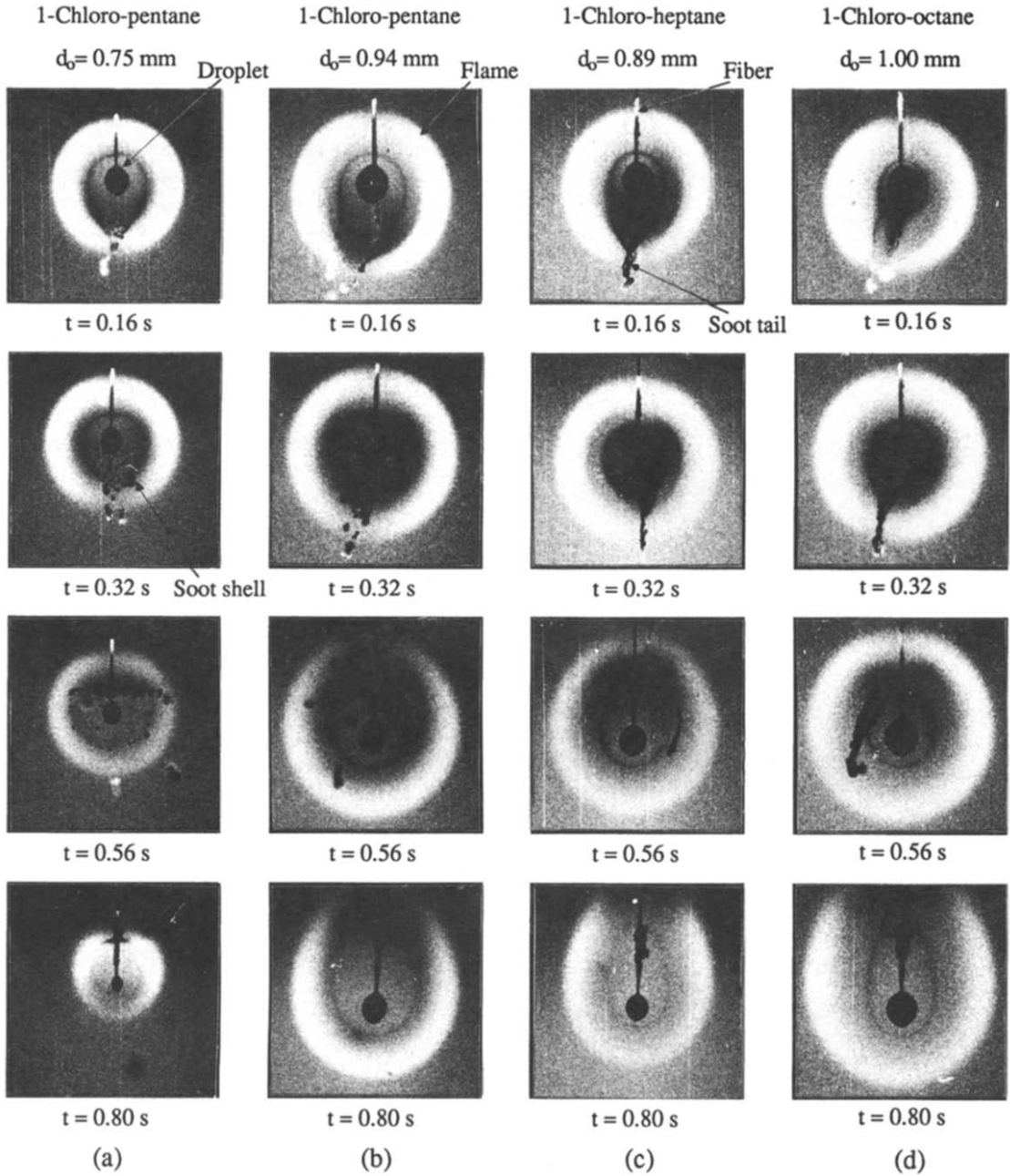
FIG. 4. Photographic sequences of pure monochloroalkane droplets suspended from a quartz fiber burning at low gravity showing the early stages of soot shell formation, the shell's increase to maximum density, and its eventual distortion due to increasing natural convection.

Table 1. Average burning rates of pure droplet fuels

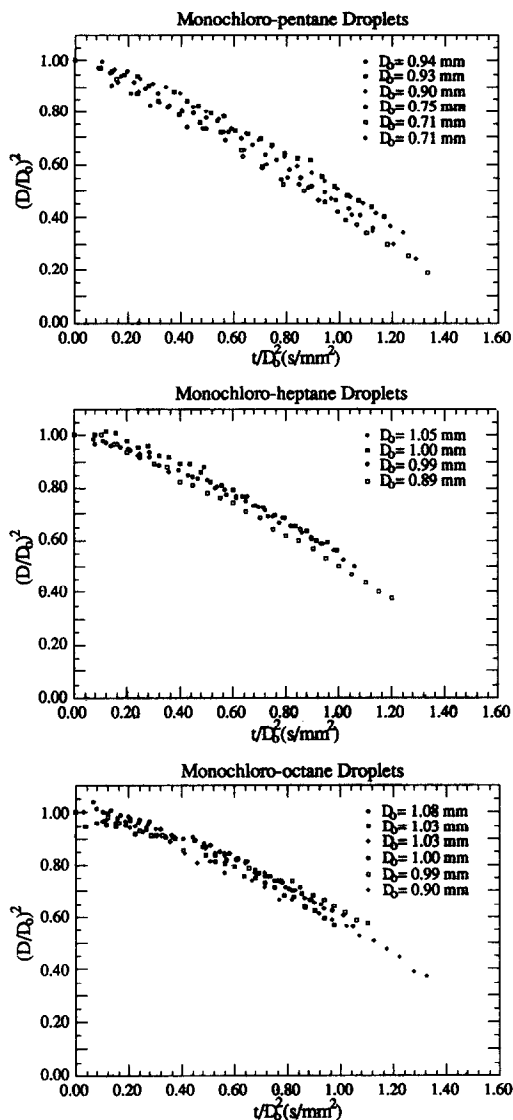| Fuel	Configuration	Runs	d_0 (mm)	w/o convection (mm^2 s^{-1})	w/convection (mm^2 s^{-1})
n-Heptane	unsupported	8	0.43–0.49	0.75 ± 0.04	—
n-Heptane	suspended	3	0.92–1.02	0.60 ± 0.01	—
1-Chloropentane	suspended	3	0.71–0.75	0.62 ± 0.03	—
1-Chloropentane	suspended	3	0.90–0.94	0.54 ± 0.03	0.65 ± 0.01
1-Chloroheptane	suspended	4	0.89–1.05	0.45 ± 0.05	0.58 ± 0.03
1-Chloro-octane	suspended	6	0.89–1.08	0.39 ± 0.04	0.54 ± 0.03

FIG. 5. Non-dimensional d^2 profiles vs time from ignition for pure monochloroalkane fuel droplets burning at low gravity.

droplet Reynolds number of about one. Such conditions, which were kept the same for each fuel, may have resulted in heated convective flows around the droplet being the dominant mode of heat transfer to the droplets and thus may have encouraged more uniform burning rates between the different fuels. In the present experiments when conditions of spherical symmetry were approximated, the dominant heat transferred to the droplet originated at the flame.

As the Grashof number increased and buoyant flows developed, the average burning rates for monochloropentane, -heptane, and -octane rose significantly, as shown in Table 1. The column labeled 'w/convection' in Table 1 lists burning rates derived from droplet diameter measurements taken from the period of combustion after buoyant flows distorted the flame and opened the soot shell. This period of transition between regimes labeled 'w/o convection' and 'w/convection' in Table 1 occurred about 0.55–0.60 s after ignition, as illustrated in the third row of photographs of Fig. 4.

The monochloroalkane droplet flames exhibited more rapid soot formation after ignition if the electric spark for ignition continued after initiation of the flame. An effect of longer spark durations on the entire combustion period, however, was not clearly visible. Not long after ignition, a soot tail formed which was sometimes pulled by gas disturbances from the downward retraction of the electrodes. The tail provided a site for further soot agglomeration as burning continued, and it resulted in emission of large soot agglomerates which passed through the flame without complete oxidation, as shown in the first two rows of photographs in Fig. 4.

The rather extensive amount of soot formed during combustion of the suspended monochloro-octane droplets provided an opportunity to gather soot agglomerates which collected on the suspension fiber during and after burning. Figure 7 shows representative transmission electron micrographs of soot agglomerates taken from a monochloroheptane flame. Approximate diameters of the individual primary particles ranged from 25 to 75 nm with an average of 45 nm. This range of soot particle sizes observed in the present experiments at low gravity was within the range of soot particle sizes noted for a wide variety of diffusion flames produced at earth's gravity as reported by Megaridis and Dobbins [11].

3.3. n-Heptane/monochloroalkane mixtures

Mixing fuels can influence the amount of soot formed and emitted from a droplet flame. To examine this effect for mixtures in which both components produce soot, mixtures of monochloro-octane and heptane were burned as suspended droplets at low gravity. Initial droplet compositions included 25%, 50%, and 75% volume by volume 1-chloro-octane in heptane.

The sooting characteristics of the mixture flames fell in between those of the pure component flames.
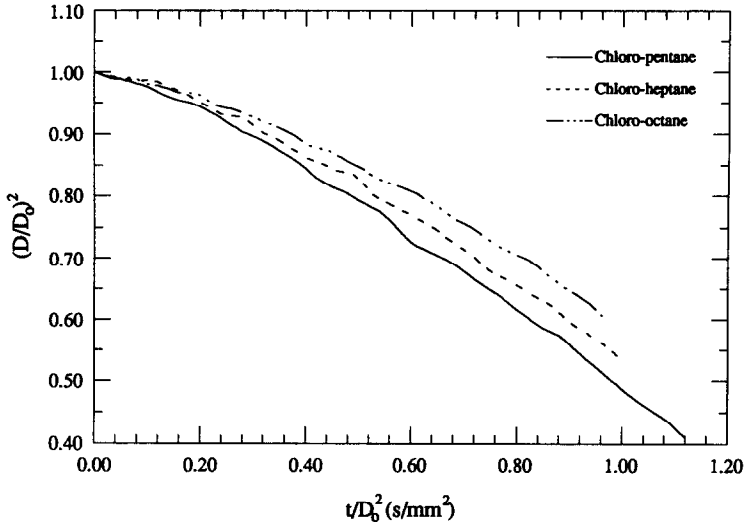
ied, Fig. 6 plots curves obtained by interpolating data of the dimensionless d^2 plots for the same fuel and then averaging the results at selected time intervals. The wavy nature of the curves in Fig. 6 is an artifact of averaging of the individual curves. The monochloropentane data used for Fig. 6 excluded data of the smaller droplets shown in Fig. 5 because they exhibited higher burning rates (cf. Section 4.4). The averaged plot reveals an initial heat-up time for each fuel as indicated by the relatively flat region in the early period of the curve.

These results may be contrasted with previous data from normal gravity experiments [10], which suggested that monochloropentane, -heptane, and -octane had nearly the same burning rate. The conditions of those experiments included a heated ambience ($\sim$900–1100 K), free-falling droplets, and a

FIG. 6. Average interpolated non-dimensional d^2 profiles vs time for the monochloroalkane droplets plotted in Fig. 5.

This fact is illustrated in Fig. 8, which shows photographic sequences of representative droplets. The initial droplet diameters to suppress possible effects of initial droplet diameter were nearly the same (cf. Section 4.4). The asymmetries in the first row of frames ($t = 0.20$ s) arose from slight disturbances in the gas flow due to electrode retraction after ignition. The second row ($t = 0.45$ s) shows the flame and soot structure near the onset of natural convection. The break-up of the soot shell by natural convection occurs earlier than for the monochloroalkane droplets shown in Fig. 4 because a longer ignition delay time was used with the mixture droplets. The third row

($t = 0.70$ s) illustrates the final distorted shape of the flame and the associated decrease in flame luminosity.

Evolutions of normalized droplet diameters for the heptane/monochloro-octane mixtures studied are shown in Fig. 9. The curves were obtained in a manner similar to those of Fig. 6. The evolutions did not markedly exhibit three-staged combustion, which is often characteristic of mixture droplet burning. Three-staged burning would be demonstrated by an intermediate period of constant droplet diameter for droplet heating. The absence of three-stage combustion suggests that the more volatile n-heptane may have been sufficiently depleted from the liquid surface during the
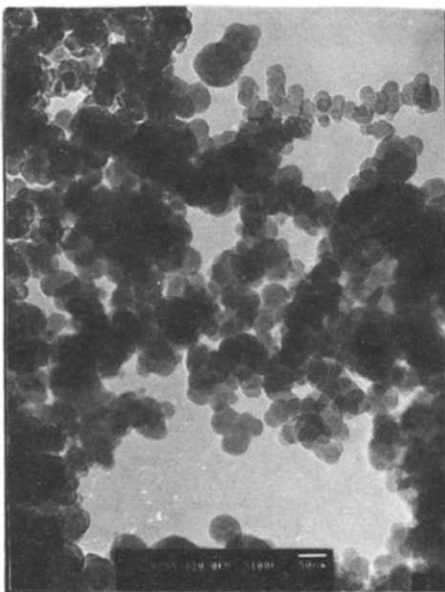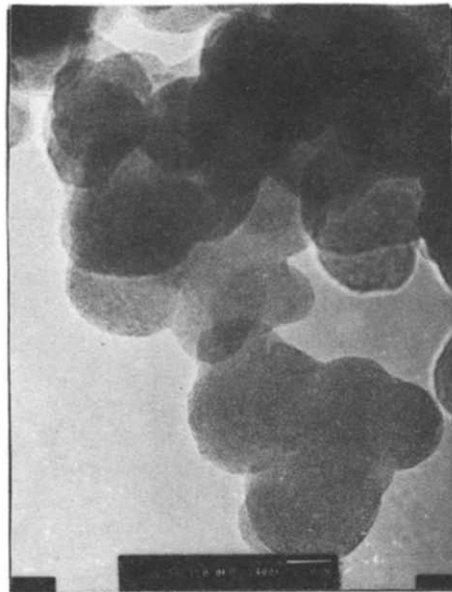
100,000 X magnification   400,000 X magnification

FIG. 7. Transmission electron micrograph of soot particles from a monochloroheptane droplet flame at low gravity.
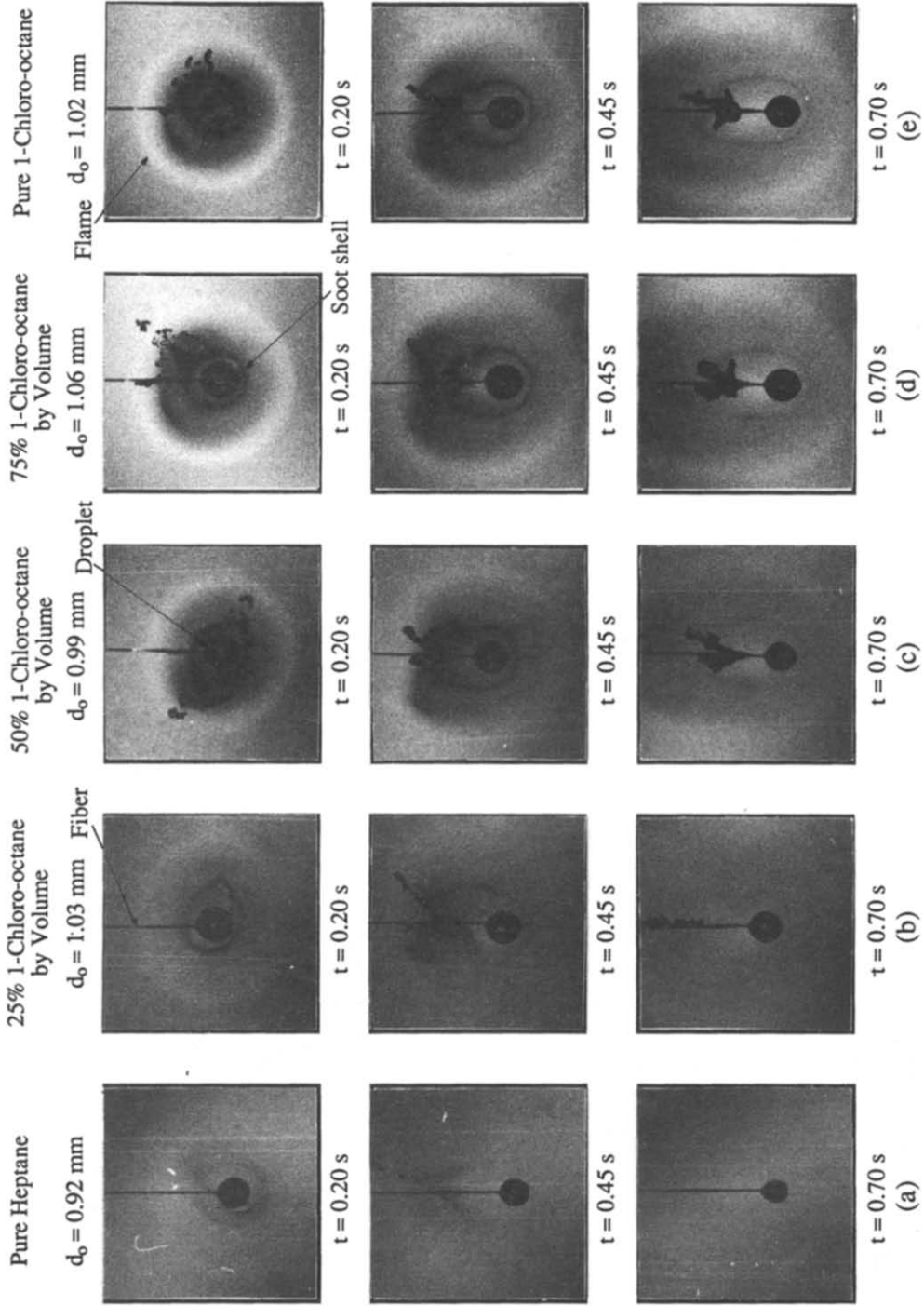
FIG. 8. Photographic sequences of suspended *n*-heptane and monochloro-octane mixture droplets burning at low gravity.
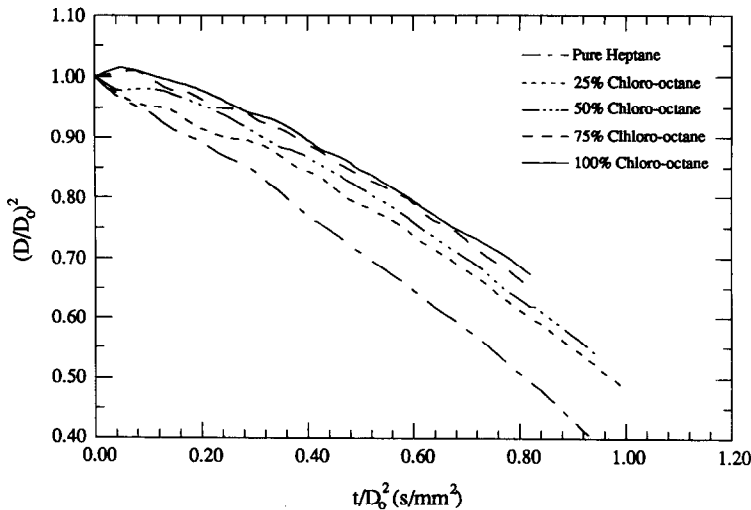
FIG. 9. Average interpolated non-dimensional d^2 profiles vs time for suspended n-heptane/monochloro-octane droplets burning at low gravity.

early stages of combustion so that further droplet heating later during combustion was not significant.

The results showed a noticeable decrease in burning rates with an increase in initial monochloro-octane concentration during the spherically symmetric phase of burning. Average burning rates for the mixtures during this period were between those of pure monochloro-octane and pure n-heptane for droplets of similar size listed in Table 1. Burning rates for the 75% mixture were well within the range of rates measured for pure monochloro-octane. Burning rates increased by over 20% for all the mixtures as natural convection distorted the flame in the latter half of combustion.

4. DISCUSSION

4.1. Soot formation in the spherically symmetric flame

The low-gravity environment may allow longer residence times for soot precursors and particles inside the droplet flame than the environment at the earth's normal gravity. This arises because axial vapor flows due to natural convection are no longer present at low gravity to sweep the soot out of the flame. Increased residence times may result in increased production of soot precursors and more accumulation of soot inside the flame. Once formed in the low-gravity flames, the soot particles experience an inwardly directed force that tends to push the particles toward the droplet as well as an outwardly directed drag force created by the Stefan flow associated with droplet vaporization. The balance of forces inside the flame promotes the formation of a shell-like structure of soot agglomerates around the droplet, which is evident in the photographs of Figs. 3, 4, and 8.

The presence of a soot shell around a burning droplet can influence the combustion process in different ways. The shell may: (1) act as a heat shield for conduction and radiation from the flame to the drop-

let, (2) reduce the mass flux of fuel from the droplet to the flame by acting as a physical barrier for mass diffusion of molecules, and/or (3) serve as a reaction site for diffusing fuel molecules. If the shell acts as a barrier to heat and/or mass transfer, then it should contribute to a lowering of the burning rate. If soot particles inside the flame become a favorable reaction site for fuel molecules, then a significant loss in the amount of fuel molecules reacting at the flame and, thus, heat generated at the flame could result from the accumulation of a shell inside the flame. Vranos and Liscinsky [12] have reported as high as 34% mass conversion of fuel molecules to soot from pyrolysis of a non-burning alkane droplet in a heated environment. If in the similar environment of droplet combustion, a comparable amount of fuel molecules produced soot inside the flame, a significant decrease in the droplet burning rate could result from the accumulation of soot inside the flame and the associated reduction in heat generated at the flame zone. Of course, if the soot is oxidized, much of its stored energy will be liberated as heat to be transferred to the droplet, but as brought out in the photographic sequences of Figs. 4 and 8, a significant amount of soot may remain inside the flame and may eventually escape the flame unoxidized.

Because the soot shell never appears to attain quasi-steady behavior in the present experiments, it is difficult to quantify its effect upon the burning rate. The soot shell does not form immediately after ignition but after a significant delay, which may signify the need for soot precursors and nucleate particles to acquire appreciable concentrations before soot agglomerates form and move in toward the droplet. As the soot moved inward from the flame boundary, it darkened due most likely to cooling. As soot collected in the shell and experienced further coagulation, the soot shell tended to increase in density while the flame remained spherically symmetric.

The extensive sooting of the monochlorinated alkanes in comparison to normal alkanes, such as heptane, reveals the strong dependence of soot formation on radicals present inside the flame zone. The chlorine radical released by the chlorinated fuels is expected to scavenge other radicals such as OH^- which are expected to inhibit the formation of soot precursors [13]. This radical scavenging results in favorable conditions for the formation of soot precursors and nucleation of soot particles in the monochloroalkane flames, and may explain the increased sooting tendencies of these fuels in comparison to normal alkanes.

4.2. Forces on soot particles inside the droplet flame

To model the soot shell in the spherically symmetric diffusion flame environment, the soot may be treated as individual particles behaving like a high molecular weight species [14] or as agglomerates behaving like an aerosol [15]. The motion of the visible soot agglomerates formed in the present study suggested that these agglomerates may have behaved like an aerosol and, therefore, that a concomitant neglect of concentration-driven diffusive transport was a reasonable assumption. The transport of soot inside the flame is then dominated by thermophoretic forces due to the temperature gradients inside the flame, as postulated for droplet combustion by Knight and Williams [16], and by the drag force due to the outwardly directed Stefan flow. A dynamic balance of the radial components of these forces on a soot agglomerate then yields

$$dU_p/d\tau = F_D + F_{TH} \equiv \zeta \tag{3}$$

where the non-dimensional radial drag (F_D) and thermophoretic (F_{TH}) forces are functions of the physical properties and the radial coordinate. The location of a stationary particle, r_{shell}, is specified by a static force balance from equation (3), which can then determine $r_{shell} \equiv r(\zeta \rightarrow 0)$.

If it is assumed that soot particles coagulate only in very small groups before collecting in the soot shell to form the chain-like connections visible in the micrographs of Fig. 7, then these agglomerates may behave similarly to single spherical particles and their motion may be modeled with previously derived expressions for F_D and F_{TH} on spherical particles. These expressions were used in order to approximate the position of mechanical equilibrium for the soot particles inside the flame. The forces were non-dimensionalized by a Millikan drag force F'_D, proportional to r_p^2. The expression for F'_D is rearranged by assuming that the mean free path is determined from its kinetic theory relationship to viscosity

$$F'_D = \frac{6\pi\mu r_p^2 v_g}{\lambda} = 3\sqrt{8\pi}r_p^2\left(\frac{R}{T}\sum_i\frac{Y_i}{W_i}\right)^{1/2}\frac{K\rho_l r_d}{8r^2}. \tag{4}$$

In order to keep the non-dimensionalizing force con-

stant, F'_D was evaluated under conditions at the droplet surface. The non-dimensional drag force on soot particles inside the flame in equation (3) was estimated by a previously suggested modification of the Millikan drag force [17]

$$F_D = \frac{F'_D}{(F'_D)_{r=r_d}}\left(\frac{1}{\left(\frac{r_p}{\lambda}+1.20+0.41\exp\left(-0.88\frac{r_p}{\lambda}\right)\right)}\right). \tag{5}$$

The non-dimensional thermophoretic force on soot particles was based on formulations derived by Talbot et al. [17], rearranged in the following form:

$$F_{TH} = \frac{F'_D}{(F'_D)_{r=r_d}}\frac{16r_d\mu}{K\rho_l}\left(\frac{dT}{dr}\right)\left(\frac{C_tC_s}{\left(\frac{r_p}{\lambda}+3C_m\right)\left(\frac{r_p}{\lambda}+2C_t\right)}\right). \tag{6}$$

Determination of the temperature gradient in equation (6) requires that the temperature field surrounding the droplet be known, which in turn necessitates a solution to the governing energy and species conservation equations. The assumption of spherical symmetry undoubtedly simplifies such a solution, but the problem is still complicated by the presence of the soot inside the flame, which is not accounted for by current droplet combustion models. In view of the fact that the purpose of the present discussion is only to show trends from a theoretical viewpoint regarding the existence of the soot shell, the temperature gradient in equation (6) is based on the classical quasi-steady spherically symmetric burning theory. The results may be expected to identify important factors upon which the existence of the shell depends. A form of the classical quasi-steady droplet burning theory which attempts to account for variations in physical properties [18] was used to determine $\partial T/\partial r$. A simplification involved neglecting the oxygen side of the flame and using the flame location and temperature as boundary conditions. A burning rate which matched experimental results was an input to determine concentration profiles and Stefan flow velocities. Temperature and concentration fields assumed that fuel, H_2O, CO_2, and N_2 were the only species present inside the flame.

The solution for $\zeta \rightarrow 0$ to find r_{shell} was obtained for conditions that attempted to match those of the suspended heptane droplets studied here and listed in Table 2. A meaningful solution is one in which

Table 2. Model conditions for n-heptane droplet burning

T_f	2300 K
K	0.6 mm^2 s^{-1}
C_{PF}	$1215 + 1.887T$ J kg^{-1} K^{-1}
$Y_{O_2,\infty}$	0.232
$Y_{N_2,\infty}$	0.768
$Y_{H_2O\infty}$	0.000
r_s	0.500 mm
r_f	3.507 mm

$r_d < r_{shell} < r_f$. The most sensitive physical property upon which a solution was found to depend was viscosity. When the viscosity [19] was calculated by neglecting fuel pyrolysis, no solution could be obtained for reasonable particle sizes. When the viscosity was arbitrarily increased by a factor of two (which, though, is not an unreasonable factor of error for the reactive multi-species environment near a flame) a solution for $\zeta \to 0$ was obtained for particles of reasonable size. Furthermore, increasing fuel diffusivity by a factor of 5 forced the model to better agree with experimentally observed values of r_f/r_d. This correction also may be reasonable because the fuel breaks into smaller molecules as it moves toward the flame and these smaller molecules may maintain higher diffusion velocities.

Figure 10 shows the variation of ζ with a dimensionless radial position inside the flame zone for a range of particle sizes. $\zeta = 0$ defines the predicted location of the soot shell for the given particle size. The results indicate that smaller soot agglomerates will tend to reside closer to the droplet than larger ones. Figure 10 further shows that the gradient of acceleration near the $\zeta = 0$ region is much higher for the smaller particles. This implies that smaller agglomerates are less likely to drift from the region of mechanical equilibrium because the forces pushing them back to equilibrium are much greater than for larger particles. Thus, smaller particles may compose a more stable shell structure.

The influence of soot agglomerate size on the shell location is further illustrated in Fig. 11, where predicted shell location is plotted against particle radius using the physical property corrections given earlier. Particularly large soot agglomerates with effective radii above 1.0 μm may not be expected to remain inside the flame ($r_{shell} < r_f$). These trends may explain the observed instability of the soot shell; as agglomerates coagulate and grow in the shell, they may

become so large that they begin to be carried back out toward the flame. These results suggest a strong link between agglomerate growth and the dynamics of soot inside the diffusion flame environment.

Figure 12 shows a comparison of the observed soot shell for a suspended n-heptane droplet with the model's predictions. The faint backlighting in the photograph provided clear visualization of the soot shell structure. This photograph is compared with the model for a droplet with the same instantaneous radius. Although the flame diameters show reasonably good agreement, the observed shell structure for the n-heptane droplets tended to be closer to the droplet surface than predicted for the physical properties used in the model. It is difficult to quantitatively compare the results of the quasi-steady model which predicts a constant shell-to-droplet diameter ratio and the unsteady results from the experimental set-up. None the less, the model does show the plausibility of the soot shell inside the droplet flame and reveals qualitative influences of various parameters upon its position.

4.3. Effect of droplet and/or gas motion on soot behavior

Both forced and natural convection influence the temperatures experienced by fuel molecules as they travel from the droplet to the flame. The significant effect of temperature upon fuel pyrolysis and thus soot formation implies that convective flows can influence soot formation. Furthermore, by carrying soot particles into the flame before they undergo significant growth, convective flows can influence soot oxidation as well. The Grashof number and the Reynolds number may be used to measure the intensity of the convective flows and thus determine the degree to which soot particles may remain inside the flame or be carried through the flame by the convective flows.

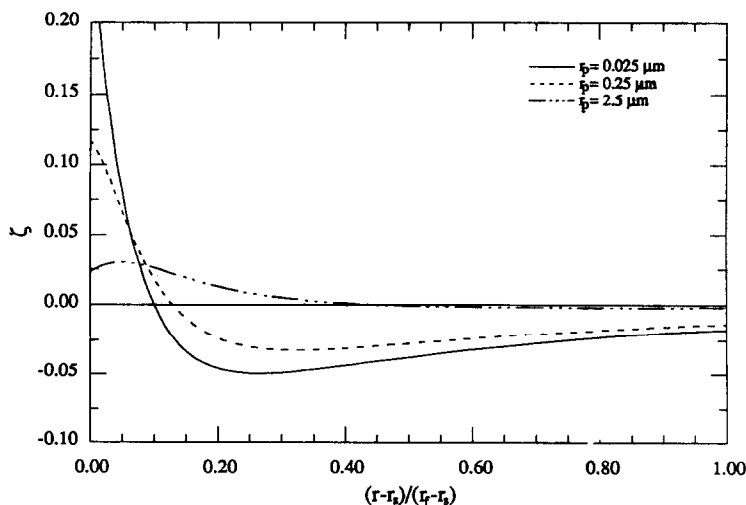Slight convective flows may dramatically reduce

FIG. 10. Plot of modeled non-dimensional net forces (ζ) vs non-dimensional radial position on stationary particles inside a spherically symmetric droplet flame (of n-heptane). Model conditions are given in Table 2.
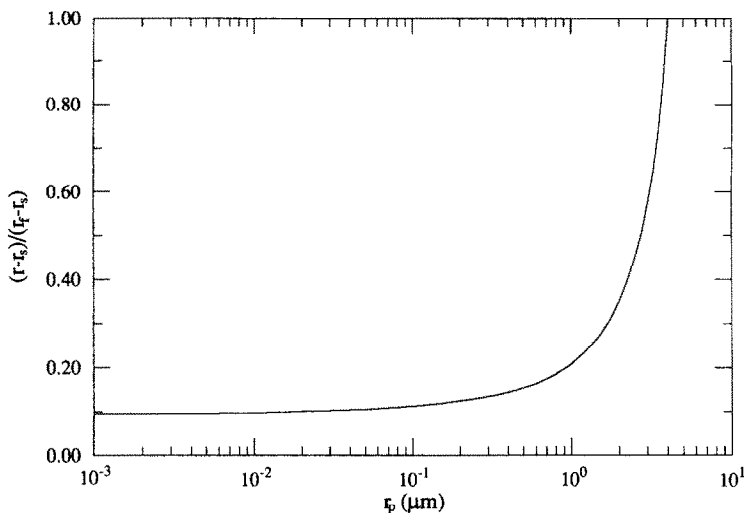
FIG. 11. Plot of predicted shell position (non-dimensionalized) with respect to size of soot agglomerates. Model conditions are given in Table 2.

soot agglomeration and soot emissions, as was observed in experiments at normal gravity [20, 21]. Soot growth and agglomeration require time for surface reaction and Brownian diffusion for coagulation. Convective flows can carry soot precursors and nucleate soot particles into the flame and thus not allow thermophoresis to keep the particles inside the flame for the extended residence times needed for soot accumulation. The decrease in luminosity of flames distorted by slight natural convective flows, as presented in the final rows of Figs. 4 and 8, indicates less soot radiation and thus likely less soot formation than with the spherically symmetric flame configuration. This reduction in soot radiation was observed for all the fuels burned in this study.

None the less, as shown in the last row of Fig. 4, the droplet flames of the highly sooting monochloroalkanes maintained distorted soot shells even under conditions of buoyant flows with Grashof numbers above 10^{-3}. Hence, even if convective flows are strong enough to open the flame, the soot agglomerates may still form and escape through the opening without significant oxidation. Thus, convective flows may aug-

ment soot emissions from highly sooting droplet flames by opening the flame and transporting soot through the opening. The present experiments with monochloroalkane droplets lend support to this notion with the observed inadequacy of convective flows in suppressing soot emissions from these fuels.

Natural convective flows can also increase vaporization rates, as clearly shown in Table 1 (cf. Section 3.2). Droplet burning rates increased when the Grashof number rose above 10^{-3} for the large suspended droplets. However, empirical correlations of droplet burning rates with Grashof number (based on the burning of less sooty normal alkane fuels) [22] predict an increase in the burning rate due to natural convection which is less than half of that observed for the heavily sooting chloroalkanes studied here. The observed increase in burning rates for the chlorinated fuels correlated with the break-up of the soot shell, which suggests that the formation of soot may have influenced the burning rates. Convective flows appeared to reduce soot accumulation. As stated earlier, unoxidized soot may have reduced the amount of fuel molecules reacting at the flame and thus the
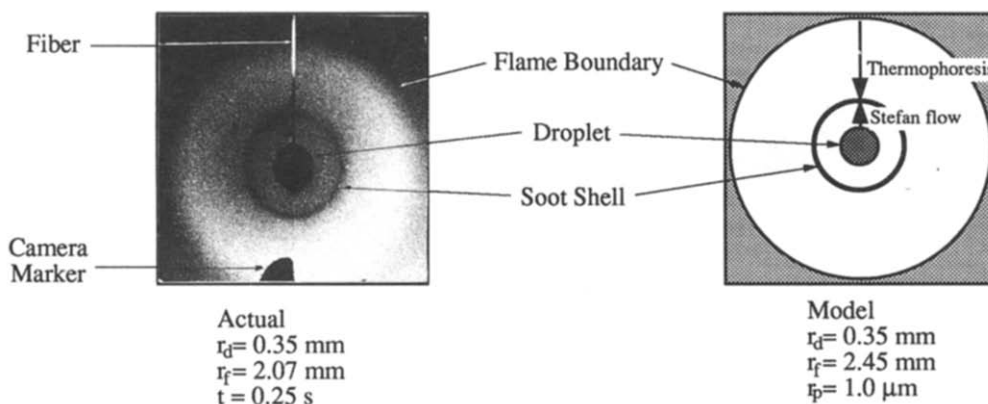

FIG. 12. Comparison of a photograph (with faint backlighting) of a suspended n-heptane droplet burning at low gravity with the theoretical model of the droplet, its soot shell, and the flame.

amount of heat generated for transfer back to the droplet. Further, the soot shell may have acted as a heat transfer barrier between the droplet and the flame in the absence of convective flows. Hence, as the shell was diminished by natural convective flows, the heat transfer from the flame to the droplet may have been promoted. This may explain the discrepancy between the correlation predictions for burning rates and the experimental results.

4.4. Effect of initial drop diameter on soot formation

Classical quasi-steady theories of droplet combustion [4] do not predict an influence of initial droplet diameter on burning. Such theories were formulated on the assumption that soot either does not form, or if it does form, that it does not play a role in the droplet burning process. However, for liquid fuels that produce soot, the present experimental results suggest an influence of initial droplet diameter. The average burning rates listed in Table 1 show that the eight small (unsupported) heptane droplets reported here burned faster (average K of 0.75 mm^2 s^{-1}) than the three large (suspended) heptane droplets (average K of 0.60 mm^2 s^{-1}). Furthermore, data during the early conditions with negligible convective flows (cf. Fig. 4) for two sets of measurements from chloropentane droplets, one with initial effective diameters in the range of 0.71–0.75 mm and the other with initial effective diameters in the range of 0.90–0.94 mm, suggest a trend that small droplets burn faster than larger droplets of the same fuel—when Re and Gr are small enough not to influence the soot dynamics. The connection between initial droplet diameter and burning rate for sooting fuels is not clearly understood, and the present discussion should only be considered as suggesting qualitative trends.

As discussed in Section 4.1, under spherically symmetric burning conditions a soot shell may influence heat and mass transfer between the flame and droplet. Generally, this impact is expected to increase with the amount of soot formed, which may be controlled in part by the residence time of fuel molecules inside the flame. Longer residence times will promote soot production and thus lower burning rates if more soot translates into reduced heat transfer to the droplet.

An approximate estimate of the residence time of fuel molecules is obtained by integrating the inverse of the average velocity derived from the classical quasi-steady burning model (which, however, neglects the presence of soot) with respect to position. It can be shown (cf. Appendix) that this residence time is proportional to the droplet size squared as given in the following expression, where $\overline{\rho_g^2 D}$ is a weighted averaged as given in the Appendix:

$$t_F = \int_{r_d}^{r_f} \frac{1}{v_g + V_F} dr = \frac{r_d^2}{(K\rho_l)^2} \overline{\rho_g^2 D}. \qquad (7)$$

Thus, fuel molecules will reside longer in high temperature regions inside the flame of larger droplets

than smaller droplets. These longer residence times could allow for more soot precursors to form, soot particles to nucleate, and agglomerates to grow by surface reactions and coagulation. The associated increase in soot formation for larger droplets may allow for thicker soot shells than for smaller droplets, with a corresponding decrease in heat transfer between the flame and droplet and hence a reduced burning rate for the larger droplets. At present, this trend of decreased burning rates with increased initial droplet size is only noted for sooting fuels which burn under conditions of negligible axial vapor flows so that combustion is primarily spherically symmetric.

5. CONCLUSIONS

The observations of soot dynamics in droplet combustion experiments performed at low gravity have provided some qualitative understanding of soot dynamics in diffusion flames. Furthermore, these experiments have provided some suggestions as to how soot formation and emissions in droplet flames are influenced by small convective flows, initial droplet diameters, and mixture compositions. It appears very likely that the variations in soot formation of different droplet sizes as well as different fuels affect the burning rates of droplets in the low-gravity environment.

The formation of a soot shell structure was observed, and its location is expected to be defined where the inwardly directed thermophoretic forces balance the outwardly directed drag forces on the soot agglomerates. A model of the spherically symmetric droplet flame, using n-heptane as the fuel, revealed that the balance of these forces was dependent upon the agglomerate size as well as physical properties of the gas mixture, in particular viscosity and fuel diffusivity. The apparent shells observed in the present experiments for n-heptane tended to be located closer to the droplet than the model predicted. The less rapid vaporization of the monochloroalkane droplets may have caused their soot shells to be closer to the droplet surface than those of n-heptane.

In general, the experiments suggest that soot formation and subsequent emissions with droplet flames can be minimized by reducing the probability of forming large soot agglomerates which can penetrate the flame without being oxidized. Reducing the formation of such agglomerates for less sooting fuels such as n-heptane may be attained with slight convective flows which distort the spherical symmetry of the flame at low gravity. On the other hand, more highly sooting fuels, such as the monochloroalkanes burned in this study, form soot agglomerates so readily that slight convective flows may rather enhance soot emissions by carrying the rapidly formed agglomerates through the distorted flame. Mixing these fuels with a less sooty fuel such as a normal alkane like n-heptane was shown to be an effective means of reducing their propensity to form soot.

REFERENCES

1. H. Hara and S. Kumagai, Experimental investigation of free droplet combustion under microgravity, *Twenty-Third Symp. (Int.) on Combustion*, The Combustion Institute, Pittsburgh, pp. 1605–1611 (1990).
2. M. Y. Choi, F. L. Dryer and J. B. Haggard, Jr., Observations on a slow burning regime for hydrocarbon droplets: *n*-heptane/air results, *Twenty-Third Symp. (Int.) on Combustion*, The Combustion Institute, Pittsburgh, pp. 1597–1604 (1990).
3. J. C. Yang, G. S. Jackson and C. T. Avedisian, Some experiments on free droplet combustion at low gravity, *AIP Conf. Proceedings 197: Drops and Bubbles*, pp. 394–403. American Institute of Physics (1989).
4. D. B. Spalding, The combustion of liquid fuels, *Fourth Symp. (Int.) on Combustion*, The Combustion Institute, Pittsburgh, pp. 847–864 (1953).
5. C. T. Avedisian, J. C. Yang and C. H. Wang, On low gravity droplet combustion, *Proc. R. Soc. Lond.* **A420**, 183–200 (1988).
6. J. C. Yang, An experimental method for studying combustion of an unsupported fuel droplet at reduced gravity, Ph.D. Thesis, Cornell University, Ithaca, NY (1990).
7. J. C. Yang, G. S. Jackson and C. T. Avedisian, Combustion of unsupported methanol/dodecanol mixture droplets at low gravity, *Twenty-Third Symp. (Int.) on Combustion*, The Combustion Institute, Pittsburgh, pp. 1619–1625 (1990).
8. S. Chandra and C. T. Avedisian, Droplet combustion near a cold surface, *Proc. R. Soc. Lond.* **A429**, 481–503 (1990).
9. T. Kadota, H. Hiroyasu and A. Farazandehemhr, Soot formation by combustion of a fuel droplet in high pressure gaseous environments, *Combust. Flame* **29**, 67–75 (1977).
10. N. W. Sorbo, C. K. Law, D. P. Y. Chang and R. R. Steeper, An experimental investigation of the incineration and incinerability of chlorinated alkane droplets, *Twenty-Second Symp. (Int.) on Combustion*, The Combustion Institute, Pittsburgh, pp. 2019–2026 (1988).
11. C. M. Megaridis and R. A. Dobbins, Morphological description of flame-generated materials, *Combust. Sci. Technol.* **71**, 95–109 (1990).
12. A. Vranos and D. S. Liscinsky, Pyrolysis of *n*-tetradecane in free droplet vaporization, *Combust. Sci. Technol.* **38**, 145–160 (1984).
13. S. M. Senkan, Combustion characteristics of chlorinated hydrocarbons. In *Detoxication of Hazardous Wastes* (Edited by J. H. Exner), Chap. 3. Ann Arbor Science, Ann Arbor (1982).
14. B. D. Shaw, F. L. Dryer, F. A. Williams and J. B. Haggard, Jr., Sooting and disruption in spherically symmetrical combustion of decane droplets in air, *Acta Astronautica* **17**, 1195–1202 (1988).
15. I. M. Kennedy, W. Kollmann and J.-Y. Chen, A model for soot formation in a laminar diffusion flame, *Combust. Flame* **81**, 73–85 (1990).
16. B. Knight and F. A. Williams, Observations on the burning of droplets in the absence of buoyancy, *Combust. Flame* **38**, 111–119 (1980).
17. L. Talbot, R. K. Cheng, R. W. Schefer and D. R. Willis, Thermophoresis of particles in a heated boundary layer, *J. Fluid Mech.* **101**, 737–758 (1980).
18. C. K. Law and H. K. Law, Quasi-steady diffusion flame theory with variable specific heats and transport coefficients, *Combust. Sci. Technol.* **12**, 207–216 (1976).
19. R. C. Reid, J. M. Prausnitz and B. E. Poling, *The Properties of Gases and Liquids* (4th Edn), pp. 392–404. McGraw-Hill, New York (1987).
20. A. L. Randolph and C. K. Law, Influence of physical mechanisms on soot formation and destruction in droplet burning, *Combust. Flame* **64**, 267–284 (1986).
21. A. Sjörgen, Soot formation of an atomized liquid fuel, *Fourteenth Symp. (Int.) on Combustion*, The Combustion Institute, Pittsburgh, pp. 919–927 (1973).
22. C. K. Law and F. A. Williams, Kinetics and convection in the combustion of alkane droplets, *Combust. Flame* **19**, 393–405 (1972).

APPENDIX

This discussion addresses the relationship between the droplet diameter and the residence time of fuel molecules in the gas phase between the droplet surface and its flame in the spherically symmetric configuration. If it is assumed that fuel molecules do not undergo any chemical reaction before reaching the flame front, the average radial velocity of the fuel molecules is then given by the sum of the Stefan flow velocity, v_g, plus the fuel diffusion velocity, V_F. An average residence time for fuel molecules in the gas phase under conditions of a spherically symmetric flame is derived by integrating the inverse of the average fuel velocity with respect to position from the droplet surface to the flame:

$$t_F = \int_{r_d}^{r_f} \frac{1}{v_g + V_F} \, dr. \tag{A1}$$

In order to simplify this integral, position is transformed into the following coordinate:

$$\xi = \exp\left(-\frac{K\rho_l}{8} \int_{r_f}^{r} \frac{r_d}{\rho_g D r'^2} \, dr' \right). \tag{A2}$$

Under conditions of spherical symmetry, an expression for v_g can be derived in terms of ξ and $d\xi/dr$

$$v_g = \frac{K\rho_l r_d}{8\rho_g r^2} = \frac{D}{\xi} \frac{d\xi}{dr}. \tag{A3}$$

Since $Y_F = 1 - \xi$ in the gas phase between the droplet and the flame, V_F is also found in terms of ξ and $d\xi/dr$

$$V_F = -D \frac{d \ln(Y_F)}{dr} = \frac{D}{1-\xi} \frac{d\xi}{dr}. \tag{A4}$$

Substituting these expressions into equation (A1) and integrating with respect to ξ gives the following:

$$t_F = \int_{\xi_d}^{1} \frac{\xi(1-\xi)}{D} \left(\frac{dr}{d\xi}\right)^2 d\xi = \int_{\xi_d}^{1} \frac{64\rho_g^2 D r^4}{(K\rho_l r_d)^2} \frac{(1-\xi)}{\xi} d\xi. \tag{A5}$$

In order to obtain the dependence of t_F on droplet size, r_d, the r inside the integral must be transformed into terms of ξ and r_d. Rearranging equation (A2) yields the following expression:

$$r = \frac{r_d}{\dfrac{r_d}{r_f} - \dfrac{8Z}{K\rho_l}}, \quad \text{when } Z = \int_{\xi}^{1} \frac{\rho_g D}{\xi'} \, d\xi'. \tag{A6}$$

From the definition of ξ given in equation (A2), it can be seen that $8Z/K\rho_l$ is simply a function of ξ. Further, in the quasi-steady analysis, r_d/r_f is constant, and the expression for r

becomes $r = r_d/f(\xi)$. Substituting equation (A6) into equation (A5) gives

$$t_F = \frac{64 r_d^2}{(K\rho_1)^2} \int_{\xi_d}^1 \rho_g^2 D f(\xi) \, d\xi. \qquad (A7)$$

The integral in the above expression can be interpreted as a weighted average value of $\rho_g^2 D$, and equation (7) is recovered

$$t_F = \frac{r_d^2}{(K\rho_1)^2} \overline{\rho_g^2 D}. \qquad (A8)$$

OBSERVATION DE LA SUIE PENDANT LA COMBUSTION D'UNE GOUTTELETTE EN FAIBLE GRAVITATION: HEPTANE ET MELANGES HEPTANE/MONOCHLORO-ALCANE

Résumé—On décrit les observations expérimentales de la combustion, avec formation de suies, des gouttes combustibles dans une tour créant un environnement à faible gravitation. Cela concerne des gouttelettes libres de n-heptane et des gouttelettes suspendues d'heptane, de monochloro-alcanes et de mélanges de monochloro-octane et d'heptane. Les diamètres initiaux des gouttelettes sont entre 0,4 et 1,1 mm. Les résultats suggèrent que la suie peut influencer la vitesse de vaporisation de la goutte. On observe de faibles courant de convection, à la fois à travers des variations de convection naturelle autour des gouttes suspendues et à travers des variations dans les vitesses des gouttes non supportées. Des faibles courants convectifs autour des gouttes suspendues réduisent la luminosité de la flamme aussi bien que l'accumulation de la suie dans la flamme et ils accroissent les vitesses de vaporisation de la goutte. Le mélange de monochloro-octane avec le n-heptane montre l'efficacité du n-heptane dans la réduction de la formation de suie dans les flammes de combustibles chlorés. On observe l'influence du diamètre initial sur la vitesse de combustion et on peut la relier à l'effet de la taille des gouttes sur la formation de suies dans les flammes.

BEOBACHTUNG VON RUSS BEI DER TRÖPFCHENVERBRENNUNG UNTER VERMINDERTER SCHWERKRAFT: HEPTAN UND GEMISCHE AUS HEPTAN UND MONOCHLORALKAN

Zusammenfassung—Es wird über experimentelle Beobachtungen bei der Verbrennung rußbildender Brennstofftröpfchen berichtet, die zur Erzeugung einer verminderten Schwerkraft in einem Fallturm durchgeführt worden sind. Es werden freie Tröpfchen aus n-Heptan betrachtet, außerdem suspendierte Tröpfchen aus Heptan, Monochloralkan und Gemischen aus beiden. Die anfänglichen Tropfendurchmesser liegen im Bereich zwischen 0,4 und 1,1 mm. Die Ergebnisse deuten darauf hin, daß der Ruß die Verdampfungsgeschwindigkeit der Tröpfchen beeinflussen könnte. Die Kugelsymmetrie der Flamme ermöglichte eine ausführliche Beobachtung der Rußanhäufungen innerhalb der Tröpfchenflamme. Außerdem wurden schwache Konvektionsströmungen beobachtet, die sowohl aufgrund der Änderung der natürlichen Konvektion um die suspendierten Tröpfchen als auch aufgrund von Änderungen der Driftgeschwindigkeit der freien Tröpfchen auftreten. Die geringe Konvektionsströmung um die suspendierten Tröpfchen reduziert sowohl die Helligkeit der Flamme als auch die Rußansammlung innerhalb der Flamme und erhöht die Verdampfungsgeschwindigkeit der Tröpfchen. Die Mischung von Monochloroktan mit n-Heptan zeigt die Wirksamkeit von n-Heptan bei der Reduktion der Rußemission in Flammen chlorierter Brennstoffe. Schließlich werden Auswirkungen des anfänglichen Tröpfchendurchmessers auf die Verbrennungsgeschwindigkeit untersucht. Diese könnten mit dem Einfluß des Tröpfchendurchmessers auf die Rußbildung innerhalb der Flamme in Verbindung gebracht werden.

НАБЛЮДЕНИЯ ЗА КОПОТЬЮ В ПРОЦЕССЕ КАПЕЛЬНОГО ГОРЕНИЯ ПРИ МАЛОЙ СИЛЕ ТЯЖЕСТИ: ГЕПТАН И СМЕСИ ГЕПТАН-МОНОХЛОРОАЛКАНЫ

Аннотация—Приводятся данные экспериментальных наблюдений за горением капель коптящего топлива, осуществляемым в капельной градирне с целью создания среды с малой силой тяжести. Исследовались свободные капли н-гептана и взвешенные капли гептана, монохлороалканов, а также смесей монохлороктана и гептана. Начальный диаметр капель изменялся в интервале 0,4–1,1 мм. Результаты показывают, что копоть может оказывать влияние на скорость испарения капель. Сферическая симметрия пламени позволила провести наблюдения за скоплениями копоти внутри него. Наблюдались также эффекты слабых конвективных течений, проявляющиеся как в изменениях естественной конвекции вокруг взвешенных капель, так и в изменениях дрейфовых скоростей свободных капель. Слабые конвективные течения вокруг взвешенных капель уменьшали яркость пламени, а также накаливание копоти в пламени и интенсифицировали испарение капель. Смешивание монохлороктана с н-гептаном продемонстрировало эффективность использования н-гептана для уменьшения выделения копоти из пламени хлорированных топлив. Кроме того, наблюдались изменения начального диаметра капель с интенсивностью горения, которые могут быть связаны с влиянием размера капли на образование копоти в пламени.